Role of Cu-Mg-Al mixed oxide catalysts in lignin depolymerization in supercritical ethanol

Role of Cu-Mg-Al Mixed Oxide Catalysts in Lignin Depolymerization in Supercritical Ethanol

AUTHOR NAMES

Xiaoming Huang,[a] *Ceylanpinar Atay,* [b] *Tamás I. Korányi,* [a] *Michael D. Boot,* [c] *and Emiel J.M. Hensen* [a,*]

AUTHOR ADDRESS

[a] Schuit Institute of Catalysis, Inorganic Materials Chemistry, Eindhoven University of Technology, P.O. Box 513, 5600 MB Eindhoven (The Netherlands),

[b] Chemical Engineering Department, Istanbul Technical University, 34469, Maslak, Istanbul, Turkey

[c] Combustion Technology, Department of Mechanical Engineering, Eindhoven University of Technology, P.O. Box 513, 5600 MB Eindhoven (The Netherlands)

[*] Correspondence to: e.j.m.hensen@tue.nl

ABSTRACT

We investigated the role of Cu-Mg-Al mixed oxides in depolymerization of soda lignin in supercritical ethanol. A series of mixed oxides with varying Cu content and (Cu+Mg)/Al ratio were prepared. The optimum catalyst containing 20 wt% Cu and having a (Cu+Mg)/Al ratio of 4 yielded 36 wt% monomers without formation of char after reaction at 340 °C for 4 h. Comparison with Cu/MgO and Cu/γ-Al_2O_3 catalysts emphasized the excellent performance of Cu-Mg-Al oxides. These mixed oxides catalyze the reaction between formaldehyde and ethanol, which limits polymerization reactions between phenolic products and formaldehyde. The combination of Cu and basic sites catalyze the associated Guerbet and esterification reactions. These reactions also protect lignin side-chains (*e.g.*, aldehyde groups). Lewis acid sites of the catalyst, mainly Cu and Al cations, catalyze C- and O- alkylation reactions that protect phenolic products and phenolic moieties in lignin oligomers. Hydrogen produced by dehydrogenation reactions is involved in hydrogenolysis reactions of the chemical bonds in lignin and also to deoxygenate the monomeric and oligomeric products. Careful investigation of the influence of the acid and base functionalities allows concluding that Guerbet and esterification reactions are more important than alkylation reactions in avoiding formation of heavy products such as char. These insights point out directions for rational design of catalysts for lignin conversion.

KEYWORDS

Lignin; catalysis; supercritical ethanol; alkylation; Guerbet reaction

1. INTRODUCTION

Lignin is a natural amorphous polymer that acts as the essential glue that gives plants their structural integrity. Along with cellulose and hemicellulose, lignin is one of the major components of lignocellulosic biomass, constituting 15-30 % of the weight and approximately 40 % of the energy content depending on the source. [1] It is the only large volume renewable feedstock that comprises aromatics. [2] For this reason and also because of its richness in functional groups, [4] lignin is a potential resource for the production of renewable fuels and chemicals. In current practice, the energy content of lignin waste produced in the paper industry is recovered by combustion and used to supply the heat required for paper pulping. With the development of second-generation bioethanol processes, it is expected that the amount of available lignin will rapidly increase. [3] This will by and large exceed the demand in current niche applications such as vanillin production and for dispersing cement. Thus, it is desirable to develop efficient catalytic processes to valorize lignin.

A variety of chemical conversion approaches such as pyrolysis, hydrocracking, hydrogenolysis, oxidation and hydrolysis have already been explored in order to convert lignin into monomeric units such as aromatics. [4] Despite significant advances made in recent years, [5-8] the selective conversion of lignin into small molecules remains a challenge. [9] This is mainly due to the recalcitrant nature and heterogeneous structure of lignin and also because the intermediates formed during its depolymerization are highly reactive, which leads to rapid repolymerization into heavier products than the starting lignin. [10,11]

Mechanistic studies have proven that repolymerization usually involves oxygenated species such as phenolic[12] and aldehyde intermediates. [10] To tackle these problems, Roberts et al. [13] explored the use of boric acid in combination with NaOH to protect the hydroxyl groups of

phenolic fragments. Barta et al. [10] demonstrated a strategy to protect reactive aldehyde fragments by reacting them with ethylene glycol to form acetals. Another undesired pathway that lowers the yield of monomers is the cross-linking of lignin fragments with formaldehyde. [3,14] Formaldehyde can be formed from lignin's native methoxy groups [15-17] as well as the γ-carbon of the alkyl side-chains in lignin. [14,18] An approach to counter these reactions is the addition of phenol to the reaction mixture, which scavenges formaldehyde and, in this way, prevents repolymerization. [14,19,20] Also radical species and unsaturated C_α=C_β side-chains were reported to play a role in repolymerization of lignin fragments. [12,21] In this case, hydrogenation of the C_α=C_β double bonds helps to reduce the negative effect of such radical reactions. [22] Reduction of oxygen functionalities also results in less reactive aromatic products such as benzene, toluene, and xylenes. [11,23,24]

Hydrogenolysis of lignin has been most frequently discussed in the scientific literature in recent years. Typically, hydrogenolysis is carried out at relatively high hydrogen pressure; in some cases hydrogen donors are used as well such as formic acid, [25,26] methanol, [6] ethanol [27,28] and *i*-propanol [7,29]. A variety of transition metals have been explored as catalysts for lignin depolymerization and the use of model compounds is often part of such investigations. Raney Ni catalyst was found to be useful in the hydrogenolysis of organosolv and Kraft lignins. [24,30,31] Wang and Rinaldi [32,33] demonstrated a catalytic process for the hydrogenolysis of model substrates, bio-oils as well as organosolv lignin involving hydrogen transfer using *i*-propanol as hydrogen donor solvent. Raney Ni was found to be very active in transfer hydrogenation and hydrogenolysis reactions for upgrading bio-oils. [30,32,33] Recently, Ni-based bimetallic catalysts, such as Ni-Au [23] and Ni-Me (Me = Ru, Rh and Pd) [34] were reported to be active for the hydrogenolysis of lignin. Multifunctional catalytic systems comprising different transition metals

and supports have also been widely investigated. [28,35-39] For instance, Song et al. [35] reported an alcoholysis-hydrogenolysis process, which yielded propylguaiacol and propylsyringol compounds in reasonable yield over a Ni/C catalyst in methanol. Ma et al. [28,38] reported on the catalytic conversion of Kraft lignin in supercritical ethanol at 280 °C using an activated carbon supported α-MoC_{1-x} catalyst. Ford and co-workers reported about a catalytic single-step deconstruction of lignin into cyclohexyl derivatives in supercritical methanol over a Cu-doped porous metal oxide catalyst at 300 °C. [29,40] At lower temperatures (140-220 °C), mainly aromatics were formed in the presence of H_2. [41] Recently, Sels presented a biorefinery process that selectively converts wood sawdust into a carbohydrate pulp and phenolic monomers-rich lignin oil in the presence of a Ru/C catalyst in methanol under H_2 atmosphere. [42] Beckham reported a supported layered-double hydroxide (LDH) containing Ni as an active component for the depolymerization of lignin model compounds as well as lignin into alkylaromatics. [43] This study pointed out the promise of LDHs as catalytically active supports in multifunctional catalyst applications. In addition to these catalyst systems, others explored the combination of supported metal catalysts with homogeneous catalysts such as mineral and Lewis acids as well as bases such as Pt/Al_2O_3-H_2SO_4, [17] Ru/C-NaOH, [44] Ni/ZSM-5-NaOH, [45] and Pd/C-$ZnCl_2$. [8] The addition of homogeneous acids or bases aids in the hydrolysis of the ether linkages to smaller fragments. [17,44] The use of basic catalysts increases the solubility of lignin. [45,46] Very recently, Abu-Omar [8] reported a synergistic Pd/C-$ZnCl_2$ system that selectively converts lignin in woody biomass into methoxyphenols in methanol, leaving behind the carbohydrates as a solid residue.

Earlier, we have reported about a one-step lignin upgrading process in supercritical ethanol using a Cu-Mg-Al mixed oxide catalyst. [27,47] This process allowed obtaining 23 wt% monomers without char formation after reaction at 300 °C for 8 h without using external hydrogen. [27] At

higher temperature (380 °C), alkylated aromatic and cyclohexanes and cyclohexenes monomer yields in the range of 60-86 wt% were obtained from organosolv, soda and Kraft lignins. [47] The oxygen-free aromatics such as benzene, toluene, and xylene and other alkylated benzenes can be used to replace reformate or serve as base aromatic chemicals; the oxygenated aromatics are prospective fuel additives with low-sooting properties and also find application as building blocks for polymers. [44] In this work, we aim at understanding the roles of the various components of the Cu-Mg-Al mixed oxide catalyst for this lignin depolymerization process. In literature, most of the investigations have been exploratory in nature with relatively little attention for understanding the role of the catalyst in the complex conversion chemistry of lignin. Especially, fundamental understanding how particular functional properties of the catalyst affect the achievable yield and the product distribution deserve more attention, because it would allow predicting catalyst-solvent combinations for improved lignin conversion. Therefore, we follow up our earlier work on mixed Cu-Mg-Al oxide catalysts for lignin upgrading[27,47] by varying the (Cu+Mg)/Al ratios and the Cu content in the hydrotalcites precursor and studying their influence on lignin conversion. XRD, N_2 physisorption, ICP and CO_2-TPD characterization were employed to investigate the physico-chemical properties of the materials. Catalyst performance data were obtained for soda lignin conversion in supercritical ethanol at 340 °C. 2D Heteronuclear Single Quantum Coherence (HSQC) NMR spectroscopy and gel permeation chromatography (GPC) were applied to follow the structural changes of lignin. In addition to lignin products, the side-products derived from ethanol conversion reactions were also analyzed. Phenol was used as a model reactant to understand the role of acid and base sites in Guerbet, esterification and alkylation reactions. Our findings will be discussed with respect to the optimum catalyst for lignin depolymerization and strategies to control the product distribution.

2. EXPERIMENTAL SECTION

2.1 Chemicals and materials

Protobind 1000 alkali lignin was purchased from GreenValue. This lignin was obtained by soda pulping of wheat straw (sulfur-free lignin with less than 4 wt% carbohydrates and less than 2 wt% ash). All commercial chemicals were analytical reagents and were used without further purification.

2.2 Catalyst preparation

Two series of Cu-Mg-Al mixed oxide catalysts with varying M^{2+}/M^{3+} atomic ratios or Cu content were obtained from calcination of Cu-doped Mg-Al hydrotalcite precursors prepared by a co-precipitation method. The catalyst samples are denoted by $Cu_xMgAl(y)$, where x corresponds to the Cu content (by weight) and y is the atomic ratio of (Cu+Mg) /Al. For example, 6 g $Cu_{20}MgAl(2)$ catalyst was prepared in the following way: 4.40 g $Cu(NO_3)_2 \cdot 2.5\ H_2O$, 15.67 g $Mg(NO_3)_2 \cdot 6H_2O$, and 15.01 g $Al(NO_3)_3 \cdot 9\ H_2O$ were dissolved in 100 ml de-ionized water. This solution in parallel with 100 ml of a NaOH (9.60 g) solution were slowly added (1 drop/sec) through 100 ml dropping funnels to 250 ml of a Na_2CO_3 (5.09 g) solution in a 1000 ml flask at 60 °C under vigorous stirring, whilst keeping the pH of the slurry at 9.5-10. When addition was complete after *ca*. 45 min, the milk-like light-blue slurry was aged at 60 °C under stirring for 24 h. The precipitate was filtered and washed with distilled water until the filtrate reached a pH of 7. The solid was dried overnight at 105 °C and grinded and sieved to a particle size below 125 μm. The hydrotalcite precursor was calcined at a heating rate of 2 °C/min from 40 °C to 460 °C and kept at this temperature for 6 h in static air. The $Cu_{20}MgO$ sample was prepared by co-precipitation in the following way: 30.31g $Mg(NO_3)_2 \cdot 6H_2O$ and 4.65 g $Cu(NO_3)_2 \cdot 2.5\ H_2O$ were

dissolved in a 150 ml de-ionized water. This solution in parallel with a 150 ml Na_2CO_3 (15.90 g) solution were slowly added in 250 ml de-ionized water in a 1000 ml flask. The pH of the slurry was kept at 8.5 under vigorous stirring at 60 °C for 3 h. The resulting precipitate was thoroughly washed with de-ionized water, dried overnight at 105 °C and calcined at 460 °C for 6 h in air. The Cu_{20}/γ-Al_2O_3 catalyst was prepared by incipient wetness impregnation using $Cu(NO_3)_2 \cdot 2.5$ H_2O precursor and a commercial γ-Al_2O_3 support (Ketjen CK 300).

2.3 Catalyst characterization

Powder X-ray diffraction (XRD) was measured on a Bruker Endeavour D4 with Cu Kα radiation (40 kV and 30 mA). They were recorded with 0.02° steps over the 5-80° angular range with 0.2 s counting time per step. N_2 physisorption was measured on a Tristar 3000 system. The samples were degassed at 300 °C for 5 h prior to measurements. The metal content of the catalysts was determined by inductively coupled plasma atomic emission spectrometry (ICP-AES) on a Spectro Ciros CCD ICP optical emission spectrometer with axial plasma viewing. All the samples were dissolved in an equivolumetric mixture of H_2O and H_2SO_4.

Temperature programmed desorption of CO_2 (CO_2-TPD) was carried out in a home-built reactor system coupled to a mass spectrometer. After pretreatment at 460 °C for 1 h in a flow of 50 mL/min He, the sample (50 mg) was cooled to 100 °C and exposed to CO_2 (25 vol% in He) for 0.5 h. After sweeping with He for 1 h to remove physisorbed CO_2, the temperature was increased linearly at a rate of 10 °C/min in He and the signal of CO_2 (M/e = 44) was recorded by online mass spectrometry (quadrupole mass spectrometer, Balzers Omnistar). The amount of CO_2 was quantified by a calibration curve, which was established by thermal decomposition of known amounts of $NaHCO_3$.

2.4 Catalytic activity measurements

The catalytic conversion of lignin and phenol were carried out in 100 ml stainless-steel high-pressure autoclaves (Parr Instrument Company). Typically, the autoclave was charged with a suspension of 0.5 g catalyst and 1.0 g feedstock (lignin or phenol) in 40 ml ethanol. The reactor was sealed and purged with nitrogen several times to remove oxygen. After leak testing, the pressure was increased to 10 bar with nitrogen and the reaction mixture was heated to 340 °C under continuous stirring at 500 rpm within 1 h. After the reaction, the heating oven was removed, and the reactor was allowed to cool to room temperature. A work-up procedure was developed to distinguish light (THF-soluble) lignin fragments and heavy (THF-insoluble) lignin fragments (THF = tetrahydrofuran) and char. A detailed description of this work-up procedure can be found in our previous report.[47]

2.5 Lignin and ethanol conversion product analysis

The liquid phase product mixture was analyzed by a Shimadzu 2010 GC-MS system equipped with a RTX - 1701 column (60 m × 0.25 mm × 0.25 μm) and a flame ionization detector (FID) together with a mass spectrometer detector. Products were identified by use of the NIST11 and NIST11s MS libraries. The peaks with the same molecular weight (M_w) were unified and presented by the structure determined by GC-MS. These products were further divided into four groups, namely hydrogenated cyclics (-O (oxygen-free)), hydrogenated cyclics (+O (oxygen-containing)), aromatics (-O) and aromatics (+O), according to the nature of the ring structure and functional groups. Semi-quantitative analysis of the liquid phase products was based on one-dimensional GC-FID analysis. Experimentally determined weight response factors of cyclohexane (1.221), cyclohexanone (0.992), ethyl benzene (1.103) and ethyl guaiacol (0.803)

were used for these four groups related to *n*-dodecane as the internal standard. The yields of lignin residue, monomers and char were calculated by using Equation (1) - (4).

Yield of monomers (wt %) =

$$\frac{\text{weight of monomers (determined by GC−FID)}}{\text{weight of starting lignin}} \times 100\% \quad (1)$$

Yield of THF-soluble LR (wt %) =

$$\frac{\text{weight of THF−soluble LR}}{\text{weight of starting lignin}} \times 100\% \quad (2)$$

Yield of THF-insoluble LR (wt %) =

$$\frac{\text{weight of THF−insoluble LR}}{\text{weight of starting lignin}} \times 100\% \quad (3)$$

Yield of char (wt %) =

$$\frac{\text{weight of char and undissolved catalyst} \times \text{weight loss in TGA}}{\text{weight of starting lignin}} \times 100\% \quad (4)$$

In order to estimate the yield of ethanol conversion products, the effective carbon number (ECN) was used to determine the relative response factors of the compounds related to *n*-dodecane as the internal standard. [48]

The gaseous products were analyzed with an Interscience Compact GC system, equipped with a Molsieve 5 Å and Porabond Q column each with a thermal conductivity detector (TCD), and an Al_2O_3/KCl column with a flame ionization detector (FID). The identification and quantification of gaseous products were done by using a gas cylinder containing known quantity of standard gas mixture.

2.6 ^{1}H-^{13}C HSQC NMR analysis

All NMR spectra were recorded using a VARIAN INOVA 500 MHz spectrometer equipped with a 5-mm ID AutoX ID PFG Probe. For the model compound sample, an aliquot of 1 ml

solution was taken from the reaction mixture followed by removing the solvent by an air flow at room temperature. The resulting mixture was dissolved in 0.7 ml dimethylsulfoxide-d_6 (DMSO-d_6). For analysis of the lignin residue, approximately 70 mg of lignin residue was dissolved in 0.7 ml DMSO-d_6. ^{1}H-^{13}C HSQC NMR spectra were obtained using the phase-sensitive gradient-edited HSQC program (gHSQCAD). The main parameters were as follows: 4 (model compound sample) or 16 (lignin residue sample) scans, acquired from 0 to 16 ppm in F2 (^{1}H) with 1200 data points (acquisition time 150 ms), 0 to 200 ppm in F1 (^{13}C) with 256 t_1 increments (acquisition time 10 ms) and 2 s relaxation delay. Data were processed using the MestReNova software. The residual DMSO solvent peak was used as an internal reference (δ_C = 39.5 ppm; δ_H = 2.50 ppm). The assignments of the cross-peaks were made by comparison with standard compounds, which contain the same functional groups (see Figure S1); the assignments beyond these standard compounds were made by use of the NMR prediction tool in ChemBioDraw Ultra 14.0.

2.7 Gel permeation chromatography (GPC)

GPC analyses were performed on a Shimadzu apparatus equipped with two columns connected in series (Mixed-C and Mixed-D, polymer Laboratories) and a UV-Vis detector at 254 nm. The column was calibrated with polystyrene standards. Analyses were carried out at 25 °C using THF as eluent with a flow rate of 1 ml/min. For the lignin residue analysis, the sample was prepared at a concentration of 2 mg/ml in THF. All the samples were filtered using 0.45 μm filter membrane prior to injection.

3. RESULTS AND DISCUSSION

3.1 Varying the M^{2+}/M^{3+} ratio

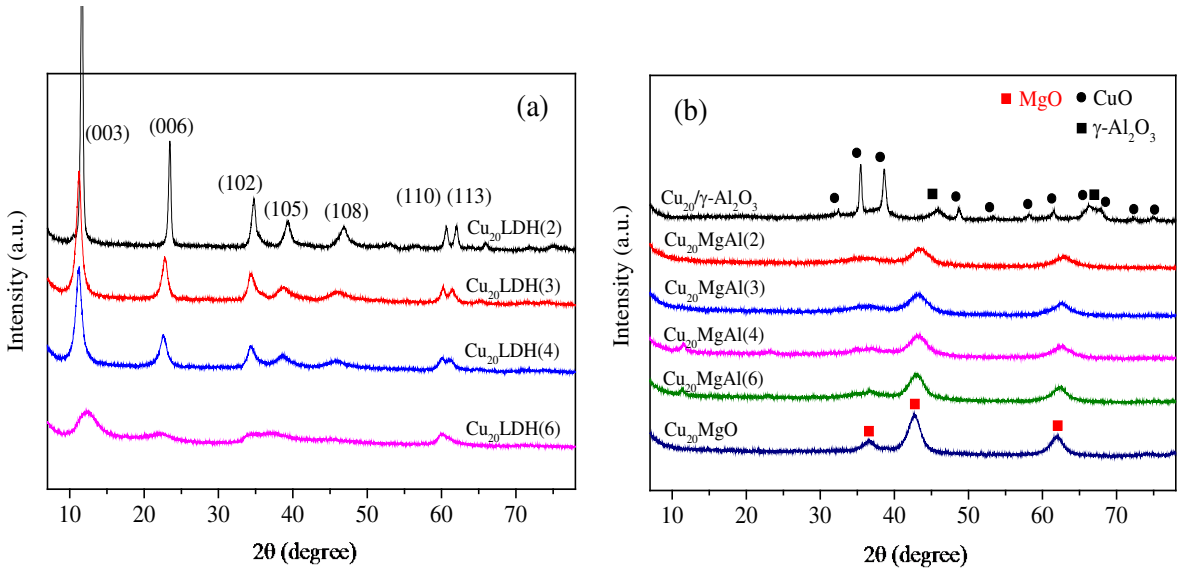

Figure 1. XRD patterns of the (a) $Cu_{20}LDH(y)$ precursors and (b) mixed oxide catalysts after calcination at 460 °C for 6 h.

Layered double hydroxides containing 20 wt% Cu, denoted by $Cu_{20}MgAl(y)$ with varying M^{2+}/M^{3+} ratios (y = 2, 3, 4 and 6), were prepared by precipitation. Mixed oxide catalysts were obtained by calcination in artificial air. Figure 1a shows the XRD patterns of the $Cu_{20}MgAl$ precursors. The patterns contain the characteristic diffraction peaks of the hydrotalcite structure. [49] The peaks become broader and less intense with increasing M^{2+}/M^{3+} ratio, which indicates that the crystallinity decreases with decreasing Al^{3+} content. The $Cu_{20}LDH(6)$ hydrotalcite shows the lowest crystallinity and, likely, contains the largest amount of amorphous material. Figure 1b shows the XRD patterns of the mixed oxides obtained by calcination of the $Cu_{20}LDH(y)$ precursors at 460 °C for 6 h. All of the $Cu_{20}MgAl(y)$ samples have the MgO structure with Cu^{2+} and Al^{3+} cations dissolved in the lattice. [50] The $Cu_{20}/\gamma\text{-}Al_2O_3$ sample prepared by impregnation shows diffraction features of the crystalline CuO phase as well as poorly crystallized $\gamma\text{-}Al_2O_3$.

The $Cu_{20}MgO$ catalyst prepared by co-precipitation also contains only MgO as crystalline phase; no other crystalline phases such as CuO and Cu^0 were observed. The presence of Cu^{2+} in the $Cu_{20}MgO$ and $Cu_{20}MgAl(4)$ samples have been confirmed by XPS (Figure S2).

Table 1. Textural properties and chemical composition of mixed oxide catalysts with different M^{2+}/M^{3+} ratios.

Catalyst	S_{BET} (m^2/g)	V^a (cm^3/g)	d^b (nm)	Cu (wt%)	Mg (wt%)	Al (wt%)	(Cu+Mg)/Al (atomic ratio)
$Cu_{20}/\gamma\text{-}Al_2O_3$	150	0.41	7.6	17.8	-	38.0	0.2
$Cu_{20}MgAl(2)$	189	0.53	15.6	16.1	21.9	14.2	2.2
$Cu_{20}MgAl(3)$	183	0.80	13.8	16.2	26.2	11.1	3.3
$Cu_{20}MgAl(4)$	206	0.72	14.9	16.3	28.3	9.1	4.2
$Cu_{20}MgAl(6)$	170	0.71	14.9	16.4	31.5	6.5	6.5
$Cu_{20}MgO$	173	0.49	10.9	20.2	33.9	-	-

[a] Average pore volume; [b] Average pore diameter.

Table 1 summarizes the textural properties and elemental composition of the mixed oxide catalyst samples. The $Cu_{20}MgAl(y)$ samples have surface areas in the 170 - 206 m^2/g range and large pore volumes (0.53 - 0.80 cm^3/g). Elemental analysis shows that the actual Cu content is slightly lower than the intended one, which is likely due to the absorption of atmospheric CO_2 and H_2O after calcination. The (Cu+Mg)/Al ratios are slightly higher than expected.

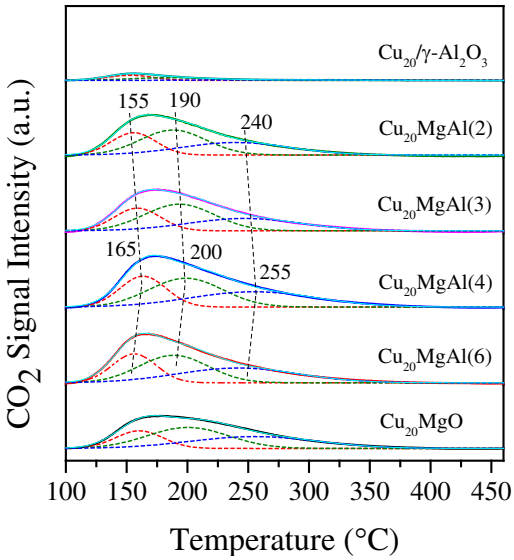

Figure 2. CO_2-TPD profiles of the mixed oxide catalysts with different M^{2+}/M^{3+} ratios.

CO_2-TPD can be used to determine the number and strength of basic sites in mixed oxides obtained by calcination of hydrotalcites. [51,52] The CO_2-TPD profiles of the catalysts are shown in Figure 2. In all cases, a broad desorption band is observed between 100 °C and 460 °C, which can be deconvoluted into three contributions at about 165 °C (weak basic strength), 200 °C (medium basic strength) and 255 °C (high basic strength).[52] The low temperature desorption peak corresponds to basic surface OH^- groups. The medium temperature peak can be ascribed to Mg^{2+}-O^{2-}, Al^{3+}-O^{2-} and Cu^{2+}-O^{2-} acid-base pairs. The high temperature peak is usually attributed to the strong basic sites associated with low coordinated O^{2-} anions. [51,52] The amount of CO_2 desorbed represented by these features allows estimating the number of basic sites of the samples (Table 2). We observe a small shift of the desorption peak towards higher temperature when the M^{2+}/M^{3+} ratio is increased from 2 to 4 (Figure 2). In addition, the total amount of basic sites of these catalysts also increased (Table 2). When the M^{2+}/M^{3+} ratio is further increased from 4 to 6, both the number of basic sites and their strength decreased. We attribute this to partial collapse of the hydrotalcite structure during synthesis of the sample with the highest M^{2+}/M^{3+} ratio in

keeping with the lowest crystallinity of this sample as followed from XRD (Figure 1a). Among all of the samples, $Cu_{20}MgAl(4)$ contains the largest amount of basic sites (0.35 mmol/g) of which weak, medium and strong basic sites account for 29 %, 38 % and 33 %, respectively. The $Cu_{20}/\gamma\text{-}Al_2O_3$ sample contains the least basic sites (0.03 mmol/g), while the $Cu_{20}MgO$ contains an intermediate amount of basic sites (0.25 mmol/g).

Table 2. Basic properties of the mixed oxide catalysts with different M^{2+}/M^{3+} ratios.

Catalyst	CO_2 desorption peaks (area %)			Total basic sites (mmol CO_2/g)
	weak (~165 °C)	medium (~200 °C)	strong (~255 °C)	
$Cu_{20}/\gamma\text{-}Al_2O_3$	46	39	14	0.03
$Cu_{20}MgAl(2)$	25	41	34	0.25
$Cu_{20}MgAl(3)$	24	43	32	0.27
$Cu_{20}MgAl(4)$	26	39	35	0.35
$Cu_{20}MgAl(6)$	26	38	36	0.31
$Cu_{20}MgO$	21	42	37	0.25

3.2 Catalytic performance in lignin conversion

Table 3. Product distribution for the reaction of lignin in ethanol at 340 °C for 4 h over mixed oxide catalysts with different M^{2+}/M^{3+} ratios.

Entry	Catalyst	Yield lignin products (wt%)					Yield ethanol products (C_{4+}, mg)				
		mono-mers	THF-soluble LR [a]	THF-insoluble LR [b]	char	total yield	alcohols	esters	aldehydes	ethers	hydro-carbons
1	Cu_{20}/γ-Al_2O_3	26	40	4	23	93	234	130	1	2490	83
2	Cu_{20}MgAl(2)	30	72	8	0	110	2276	776	32	103	193
3	Cu_{20}MgAl(3)	31	75	8	0	114	2348	663	40	125	317
4	Cu_{20}MgAl(4)	36	69	6	0	110	3214	1069	67	105	336
5	Cu_{20}MgAl(6)	31	70	7	0	108	2996	695	31	153	300
6	Cu_{20}MgO	20	47	15	0	82	2722	371	96	51	155

[a] Relatively light lignin fragments with molecular weight lower than starting lignin, [b] Heavy lignin fragments.

We evaluated these samples as catalysts in the conversion of soda lignin in supercritical ethanol at a temperature of 340 °C and a reaction time of 4 h. We have chosen soda lignin, because it is one of the few commercially available lignins together with lignosulfonates and Kraft lignin.[53] Soda lignin is free from sulfur and relatively pure, which are ideal properties for the present detailed mechanistic study. The results of the reaction experiments with soda lignin are collected in Table 3. As described earlier, lignin is partially depolymerized and the products are further converted by alkylation, hydrodeoxygenation and hydrogenation reactions. [27,47] Ethanol acts as an efficient alkylation agent. At the same time, ethanol reacts itself to higher alcohols, esters, aldehydes, ethers and a small amount of hydrocarbons (Table S1). The ethanol conversion products were identified by carrying out the same reaction without lignin under similar conditions (Table S2). It was observed that molecules with hydrocarbon rings were derived from lignin and acyclic hydrocarbons stemmed from ethanol. As an example, for

$Cu_{20}MgAl(4)$ about 84 lignin products and 48 ethanol-derived products were identified by GC-MS. Without catalyst, lignin was only partially depolymerized and the main product was char with only a small amount of monomers (Table S3). [27]

All the basic catalysts produce high yields of C_{4+} alcohols and esters (entries 2-6). These products are formed via Guerbet-type reactions as well as esterification reactions, which are all catalyzed by basic sites. [54] For example, when $Cu_{20}MgAl(4)$ was used as the catalyst (entry 4), 3214 mg of higher alcohols and 1069 mg of higher esters were obtained. The most significant products were 1-butanol, 2-buten-1-ol, 1-hexanol, ethyl acetate and acetaldehyde. Among the C_{4+} molecules, 1-butanol and ethyl acetate were dominant with selectivities of 47 wt% and 13 wt%, respectively. On contrary, with $Cu_{20}/\gamma\text{-}Al_2O_3$ only comparatively small amounts of higher alcohols and esters were formed. The difference can be related to the low basicity of the alumina-supported Cu catalyst (Table 2). In this experiment, the amount of C_{4+} ethers was high; about 81% of these ethers was diethyl ether. Diethyl ether is formed by dehydration of two ethanol molecules, which is typically catalyzed by acid sites as present on the surface of alumina. [51,55] Comparison of the ethanol conversion products (Table 3) with the catalyst properties (Table 2) shows a strong correlation between the basic sites and the overall yield of alcohols and esters. The higher the basicity of the catalyst is, the higher the amount of alcohols and esters formed via Guerbet-type and esterification reactions. [54,56]

In addition to cyclic products obtained from lignin, the reaction mixture also contained THF-soluble LR, THF-insoluble LR and char. Figure S3 shows a typical GPC-derived molecular-weight distribution of the P1000 lignin and the two different lignin residues obtained with $Cu_{20}MgAl(2)$ as the catalyst (Table S4). The weight-averaged molecular weight (M_w) of the THF-soluble fraction is 817 g/mol, which is lower than the THF-soluble fraction of P1000 lignin

(M_w = 1104 g/mol). The THF-soluble LR represents fragments of lignin that have been depolymerized to lower molecular weight. [27] These fragments are extensively alkylated as reported earlier. [27] The THF-insoluble residue shows a broad peak at early elution times. The M_w of this residue is 8479 g/mol (Table S4), much higher than that of the starting lignin. The heavier molecules originate from condensation reactions between lignin fragments. Finally, char is characterized by the fraction that is strongly adsorbed to the solid catalyst; it had the lowest H/C ratio of the different solid fractions. [27] From Table 1, it follows that the use of the non-basic Cu_{20}/γ-Al_2O_3 catalyst results in a significant amount of char (23 wt%, entry 1). On contrary, the use of basic catalysts did not lead to char formation (entries 2-6). Thus, it can be inferred that the basic sites of the hydrotalcites-derived mixed oxides play an important role in preventing char formation. The beneficial effect of bases such as NaOH during lignin conversion has been recognized before. [13,46] The usual explanation is that the base helps to increase solubility of lignin, resulting in a better dispersion and lower probability of recombination reactions. [13,46] The influence of base-catalyzed side-reactions such as Guerbet and esterification reactions has only been scarcely discussed. Recently, we have demonstrated that methanol and formaldehyde are effectively scavenged by reaction with ethanol. [47] The main product from the reaction between ethanol and formaldehyde is *n*-propanol. In this way, ethanol can effectively suppress repolymerization reactions involving formaldehyde, which can be formed in a variety of manners from the lignin structure. In line with this, the most basic Cu_{20}MgAl(4) sample gave also the highest yield of ethanol-derived products and the lowest yield of THF-insoluble LR (8 wt%, entry 4).

Although Cu_{20}MgO contains basic sites and produces similar Guerbet and esterification reaction products (entry 6) compared with Cu_{20}MgAl(2) (entry 2) and Cu_{20}MgAl(3) (entry 3), its

THF-insoluble LR yield is significantly higher. We relate this to different rates of the alkylation reactions of the aromatic products, which also contribute to suppressing repolymerization reactions. [27,47] It is reasonable to postulate that the lower alkylation activity is associated with the absence of Al. It is well known that alkylation reactions (*e.g.*, phenol alkylation with alcohols) are catalyzed by inorganic Lewis and/or Brønsted acids such as H_2SO_4, $AlCl_3$, BF_3, [57] as well as solid acids such as zeolites. [58]

In order to establish whether differences in the alkylation activity can explain the better performance of the hydrotalcites derived catalysts, we carried out model reactions using phenol as reactant in supercritical ethanol (340 °C, 4 h, 1 g phenol, 40 ml ethanol). The reaction mixtures were analyzed by GC-MS and quantified by GC-FID. The reaction mixtures were further analyzed by 2D HSQC NMR. Semi-quantitative analysis was achieved by integrating the C- and O-ethylated product peaks (-CH_2 group) using the DMSO-d_6 residual solvent peak as the internal standard (Figure 3). The resulting value reflects the degree of phenol alkylation.

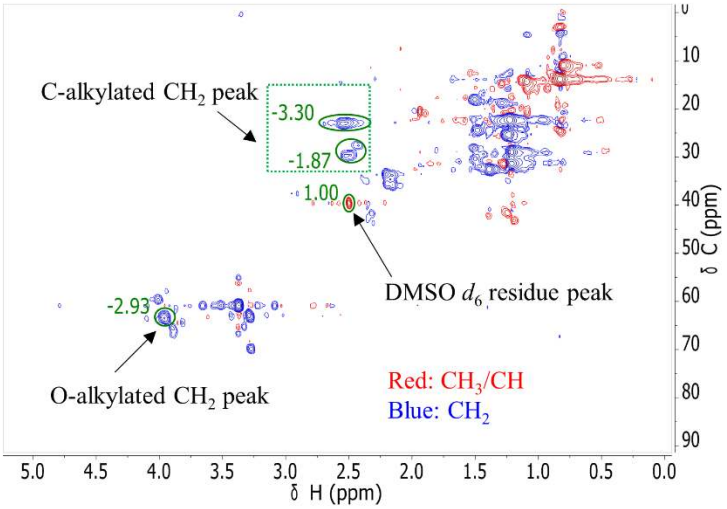

Figure 3. Side-chain region of the ^{1}H-^{13}C HSQC NMR spectrum of the reaction mixture obtained by reaction of phenol in ethanol at 340 °C for 4 h over the Cu_{20}/γ-Al_2O_3 catalyst.

The alkylation degree of $Cu_{20}MgO$ is 2.4 (Table 4). This value is much lower than the phenol alkylation degree using the Al-containing $Cu_{20}MgAl(y)$ catalysts, which had values between 3.3 and 5.4 (Table 4). In line with this, the $Cu_{20}MgO$ sample gave the lowest yield of alkylated products (48 wt%) of which more than half are mono-alkylated products (28 wt%). The Al-containing $Cu_{20}MgAl(y)$ catalysts gave much higher yields of alkylated products (between 61 wt% and 69 wt%), about half of which are multi-alkylated products. The $Cu_{20}/\gamma\text{-}Al_2O_3$ sample gave the highest alkylation degree of 8.1 and the highest alkylated product yield of 81 wt% (Table 4); the yield of multi-alkylated products is 58 wt%. Thus, the alkylation activity strongly correlates with the Al content (Table 4). The higher the Al content is, the higher the degree of alkylation of phenol. Although $Cu_{20}/\gamma\text{-}Al_2O_3$ has the highest alkylation activity, its performance in lignin conversion is worse than that of $Cu_{20}MgAl(4)$. Thus, we infer that Guerbet and esterification reactions are more important than alkylation in suppressing char formation. This emphasizes the role of formaldehyde in the condensation reactions that give rise to high-molecular weight side-products. [47]

Table 4. Phenol alkylation in ethanol at 340 °C for 4 h over the mixed oxide catalysts with different M^{2+}/M^{3+} ratios.

Catalyst	X (wt%) [a]	Yield of alkylated products (wt%) [a]			Alkylation degree [b]
		mono-alkylated	multi-alkylated	sum	
$Cu_{20}/\gamma\text{-}Al_2O_3$	85	23	58	81	8.1
$Cu_{20}MgAl(2)$	72	34	35	69	5.4
$Cu_{20}MgAl(3)$	70	33	32	65	3.7
$Cu_{20}MgAl(4)$	69	30	34	64	3.4
$Cu_{20}MgAl(6)$	64	30	31	61	3.3

Cu_{20}/MgO	56	28	21	49	2.4

[a] Conversion determined by GC-FID using area normalization method, [b] Determined by ^{1}H-^{13}C HSQC NMR using DMSO d_6 residue peak as internal standard.

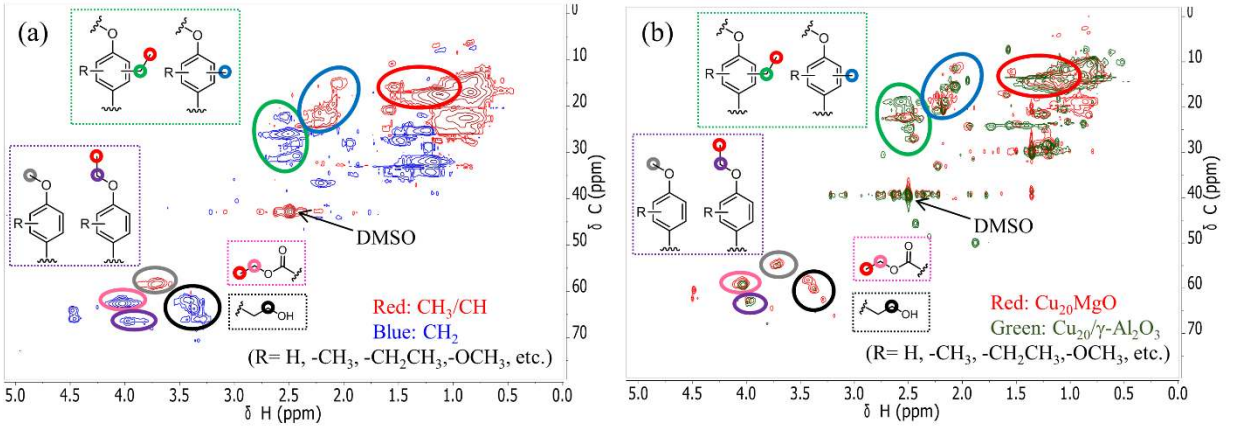

Figure 4. The side-chain region of the ^{1}H-^{13}C HSQC NMR spectrum of the THF-soluble LR obtained from the reaction in ethanol at 340 °C for 4 h for (a) Cu_{20}MgAl(4) and (b) Cu_{20}MgO (red) and Cu_{20}/γ-Al_2O_3 (green). The combined spectra in panel (b) have been normalized to the total peak volume.

In comparing the THF-soluble LR yields and the total yield, the THF-soluble LR yields are between 69 and 75 wt% and the total yields are between 108 and 114 wt% for the Cu_{20}MgAl(*y*) catalysts. The high yields of THF-soluble LR and higher than 100% total yields are due to the significant degree of alkylation of the lignin-derived products. Figure 4a shows the HSQC NMR spectrum of the THF-soluble LR obtained from the reaction over the Cu_{20}MgAl(4) catalyst. Significant alkylation of aromatic rings and phenolic groups is evident. A high amount of C- and O-ethylated products were formed, which proves that ethanol alkylates the lignin fragments. A significant number of cross peaks due to ester and alcohol groups are also seen, which indicates that Guerbet and esterification reactions took place between hydroxyl and aldehyde groups of the lignin fragments and ethanol. These reactions are important, because aldehyde intermediates are

known to play a significant role in aldol condensation reactions during lignin depolymerization. [10] For instance, Barta et al. [10] demonstrated a novel strategy to stabilize these reactive aldehyde fragments (C_2-aldehyde) by reacting them with ethylene glycol to form acetals. The formation of higher molecular weight side-products was markedly suppressed in this way. The importance of these reactions in our approach is underpinned by the absence of ^{1}H NMR signals related to aldehyde groups in the spectrum of the THF-soluble LR obtained by reaction at 340 °C for 4 h over Cu_{20}MgAl(4). Consistently, very few aldehyde products were formed from ethanol conversion (Table 3). These results indicate that aldehyde groups can be effectively capped by ethanol via Guerbet and esterification reactions. Figure 4b shows the NMR spectra of the THF-soluble LRs obtained from lignin conversion using Cu_{20}/γ-Al_2O_3 and Cu_{20}MgO catalysts. With Cu_{20}/γ-Al_2O_3, more ethylated groups but much less ester and alcohol groups were formed as compared with Cu_{20}MgO. This finding is consistent with the activity differences based on the yields of ethanol-derived products in lignin conversion. The low alkylation activity of Cu_{20}MgO, on the one hand, and the low Guerbet and esterification activities of Cu_{20}/γ-Al_2O_3, on the other, explain the lower THF-soluble LR yields compared with the performance data for the Cu_{20}MgAl(*y*) catalysts. Thus, we attribute the promising performance of Cu_{20}MgAl(*y*) catalysts in terms of high monomers yield and low yield of repolymerized products during lignin depolymerization to their high activity in Guerbet, esterification and alkylation reactions.

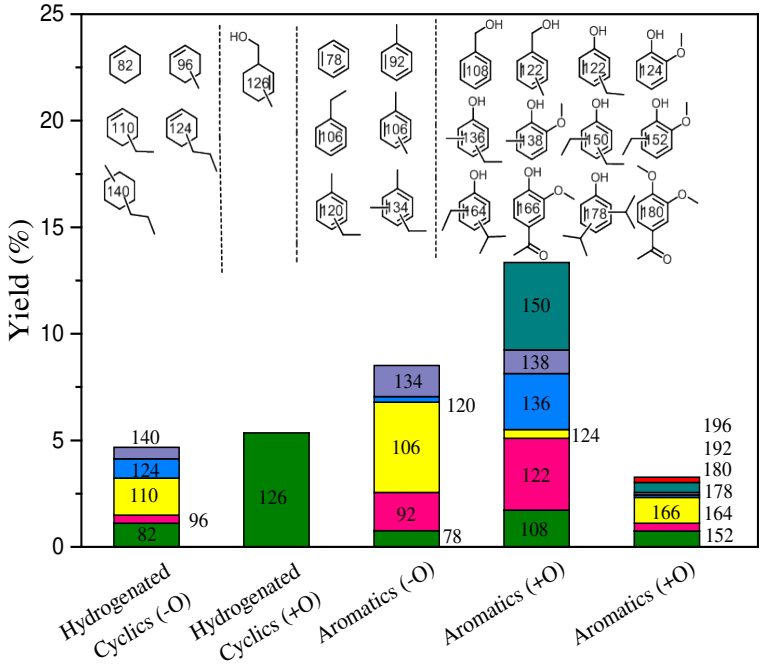

Figure 5. Distribution of lignin monomers after reaction of lignin at 340 °C for 4 h over $Cu_{20}MgAl(4)$.

Figure 5 shows a typical lignin-derived product distribution of the monomer fraction of the products obtained after reaction at 340 °C for 4 h over $Cu_{20}MgAl(y)$. The main products were aromatics with hydrogenated cyclic products as the main side-products. Most of these products were alkylated with methyl and/or ethyl groups substituted on the rings. Notably, a substantial amount of deoxygenated aromatics such as benzene, toluene, xylenes, and ethyl benzene were observed, pointing to direct hydrogenolysis of the aryl-OR bonds (R = alkyl). The most frequently observed oxygenated aromatics were substituted benzylalcohols and alkylphenols. Besides, small amount of guaiacols were observed among the products. The monomeric products were divided into four groups, namely hydrogenated cyclics (-O), hydrogenated cyclics (+O), aromatics (-O) and aromatics (+O).

Figure 6 shows the trends in monomers yield and the product selectivity among the different catalysts. Using $Cu_{20}/\gamma\text{-}Al_2O_3$, the amount of monomers was 26 wt%. Increasing the M^{2+}/M^{3+} ratio in the LDH precursor (entries 2-6) led to higher monomers yields. The highest monomers yield of 36 wt% was obtained with $Cu_{20}MgAl(4)$. $Cu_{20}MgO$ gave the lowest monomers yield (20 wt%). The product distributions of the monomers were quite similar among the $Cu_{20}MgAl(y)$ catalysts. $Cu_{20}MgAl(4)$ showed slightly higher selectivity towards deoxygenated aromatics than the other $Cu_{20}MgAl(y)$ (y = 2, 3 and 6) catalysts. This indicates that the $Cu_{20}MgAl(4)$ catalyst has the highest deoxygenation activity. This is likely due to the larger amount of H_2 formed (34.76 mmol) from ethanol dehydrogenation (Table S5). Hydrogenation is needed for the direct hydrogenolysis reactions of aryl-OR bonds. In line with this, the $Cu_{20}/\gamma\text{-}Al_2O_3$ catalyst, which exhibited the lowest dehydrogenation activity (7.59 mmol H_2 production, Table S5) gave the highest selectivity towards oxygenated aromatics (~ 83% in the monomers mixture).

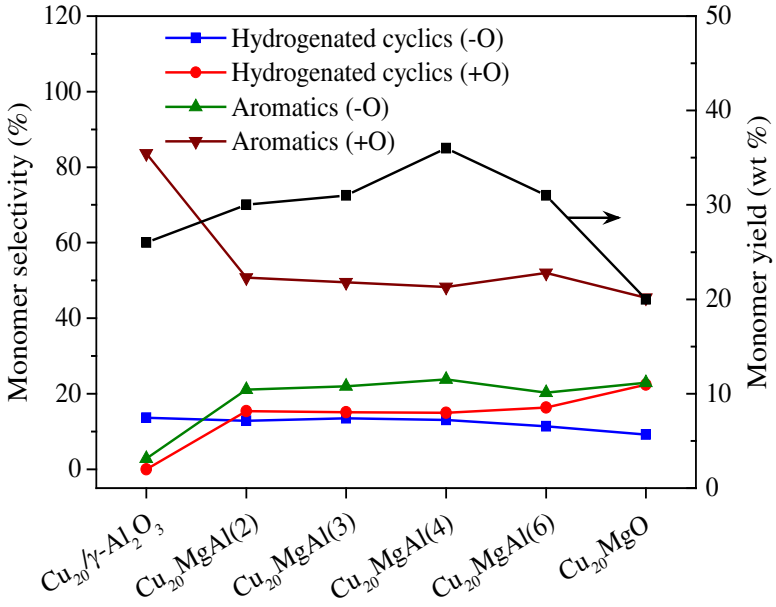

Figure 6. Monomers yield and product selectivity after lignin conversion in ethanol at 340 °C for 4 h over mixed oxide catalysts as a function of the M^{2+}/M^{3+} ratio**.**

3.3 Varying the Cu content

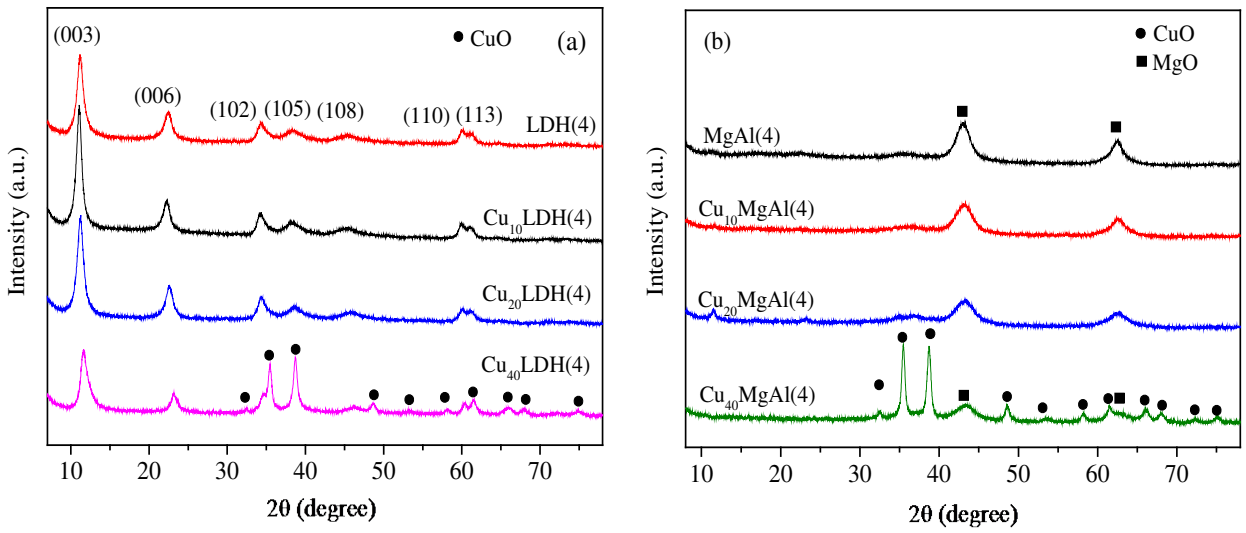

Figure 7. XRD patterns of (a) the $Cu_xLDH(4)$ precursors and (b) mixed oxides after calcination at 460 °C for 6 h.

In order to better understand the role of Cu, we varied the Cu content (0 wt%, 10 wt%, 20 wt% and 40 wt%) in the MgAl(4) precursor and obtained mixed oxide catalysts by calcination. The M^{2+}/M^{3+} atomic ratio of 4 was chosen, because the highest monomers yield was achieved at this composition during lignin conversion. Figure 7a shows the XRD patterns of the $Cu_xLDH(4)$ precursors. The pattern of the Cu-free precursor contains the characteristic peaks corresponding to hydrotalcite. Partially replacing Mg by 10 wt% or 20 wt% of Cu did not notably change the double-layered structure. However, further increasing the Cu content to 40 wt% resulted in the formation of CuO and, at the same time, lower intensities of the peaks due to the hydrotalcite structure. This indicates that too high Cu content resulted in the partial collapse of the hydrotalcite structure. Figure 7b shows the XRD patterns of the mixed oxides obtained by calcination of the corresponding hydrotalcite precursors. The MgAl(4), Cu_{10}MgAl(4) and

$Cu_{20}MgAl(4)$ samples all have the MgO structure. In $Cu_{40}MgAl(4)$, both MgO-like and CuO crystalline phases were present.

Table 5. Textural properties and chemical composition of the mixed oxides as a function of the Cu content.

catalyst	S_{BET} (m^2/g)	V [a] (cm^3/g)	d [b] (nm)	Cu (wt%)	Mg (wt%)	Al (wt%)	(Cu+Mg)/Al (atomic ratio)
MgAl(4)	245	0.82	13.0	-	36.50	9.77	4.20
$Cu_{10}MgAl(4)$	240	0.73	12.1	8.08	33.64	9.66	4.27
$Cu_{20}MgAl(4)$	206	0.72	13.8	16.33	28.30	9.13	4.24
$Cu_{40}MgAl(4)$	125	0.56	24.5	31.43	16.67	7.54	4.25

[a] Average pore volume, [b] Average pore diameter.

Table 5 summarizes the textural properties and elemental composition of the mixed oxides. The MgAl(4) sample has the highest surface area (245 m^2/g) and pore volume (0.82 cm^3/g). The replacement of Mg by Cu to yield 10 wt% and 20 wt% Cu led to only slightly lower surface areas and pore volumes. At the highest Cu content, the surface area was much lower (125 m^2/g), which can be related to the collapse of the hydrotalcite structure of the precursor (Figure 7). The (Cu+Mg)/Al ratios in the calcined samples were between 4.20 and 4.27.

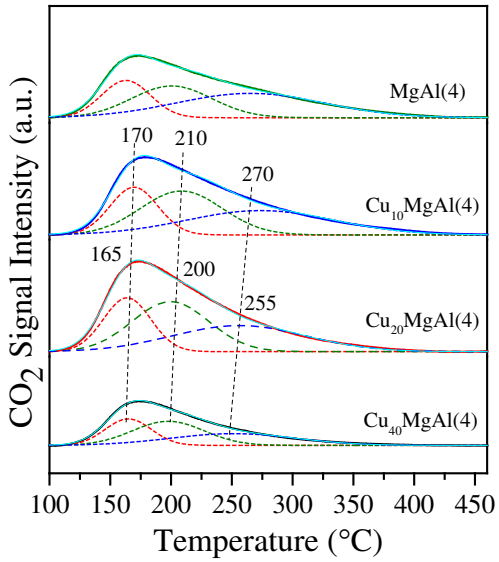

Figure 8. CO_2-TPD profiles of the mixed oxide catalysts as a function of the Cu content.

Table 6. Basic properties of the mixed oxide catalysts as a function of the Cu content.

Catalyst	CO_2 desorption peaks (area %)			Total basic sites (mmol CO_2/g)
	weak (~165 °C)	medium (~200 °C)	strong (~255 °C)	
MgAl(4)	20	28	52	0.27
Cu_{10}MgAl(4)	24	38	38	0.32
Cu_{20}MgAl(4)	29	38	33	0.35
Cu_{40}MgAl(4)	30	39	31	0.15

The CO_2-TPD profiles of the catalysts are shown in Figure 8. The number of basic sites and basic sites densities are shown in Table 6. The Cu-free catalyst (MgAl(4)) mainly contains medium (28 %) and strong basic sites (52 %). With increasing Cu content, the amount of strong basic sites decreases, while the amount of weak and medium basic sites increased (Table 6). Consistently, the desorption peak shifted to lower temperatures (Figure 8). The amount of basic

sites was seen to increase with increasing Cu content up to 20 wt% (Table 6) at the expense of their strength. A further increase of the Cu content to 40 wt% resulted in a significant decrease of the amount of basic sites, probably due to the formation of CuO as a result of the collapse of the hydrotalcite precursor.

Table 7. Product distribution for the reaction of lignin in ethanol at 340 °C for 4 h over the mixed oxide catalysts as a function of the Cu content.

Entry	Catalyst	Yield lignin products (wt%)					Yield ethanol products (C_{4+}, mg)				
		mono-mers	THF-soluble LR [a]	THF-insoluble LR [b]	char	total yield	alcohols	esters	aldehydes	ethers	hydro-carbons
1	MgAl(4)	9	42	15	0	66	1343	150	10	247	102
2	Cu_{10}MgAl(4)	21	61	13	0	95	2471	506	36	123	127
3	Cu_{20}MgAl(4)	36	69	6	0	110	3214	1069	67	105	336
4	Cu_{40}MgAl(4)	26	79	8	0	113	2372	593	80	116	254

[a] Relatively light lignin fragments with molecular weight lower than starting lignin, [b] Heavy lignin fragments.

Using the Cu-free MgAl(4) sample as the catalyst, the monomers yield is only 9 wt% with the major products being THF-soluble LR (42 wt%) and THF-insoluble LR (15 wt%) (Table 7). The total yield in this case is 66%. We speculate that the low total yield is due to the low rates of Guerbet, esterification and alkylation reactions in the absence of Cu. Based on our experimental observations, part of the lignin fragments - likely dimers and trimers - could not be completely recovered during the acidification and filtration steps of the work-up procedure.[47] We expect that this loss will be lower when lignin has been extensively alkylated, as the heavier and more apolar compounds will be less soluble in ethanol. Consistent with this, the yield of THF-soluble LR and the total yield increased when the rates of Guerbet, esterification and alkylation reactions

catalyzed by Cu were enhanced by increased Cu content. In keeping with this conclusion, the alkylation degree obtained from phenol alkylation model experiments also increased with the Cu content (Table 8). For example, the alkylation degree of $Cu_{40}MgAl(4)$ is 5.9, which is significantly higher than that of MgAl(4). Besides, GC-MS results also show that significant higher yields of multi-alkylated products (42 wt%) were obtained with $Cu_{40}MgAl(4)$ as the catalyst as compared with MgAl(4). This implies that Cu and Al sites are both key to catalyze alkylation reactions and it is reasonable to state that these sites constitute Lewis acid sites for aromatics alkylation. The optimum Cu content is 20 wt%.

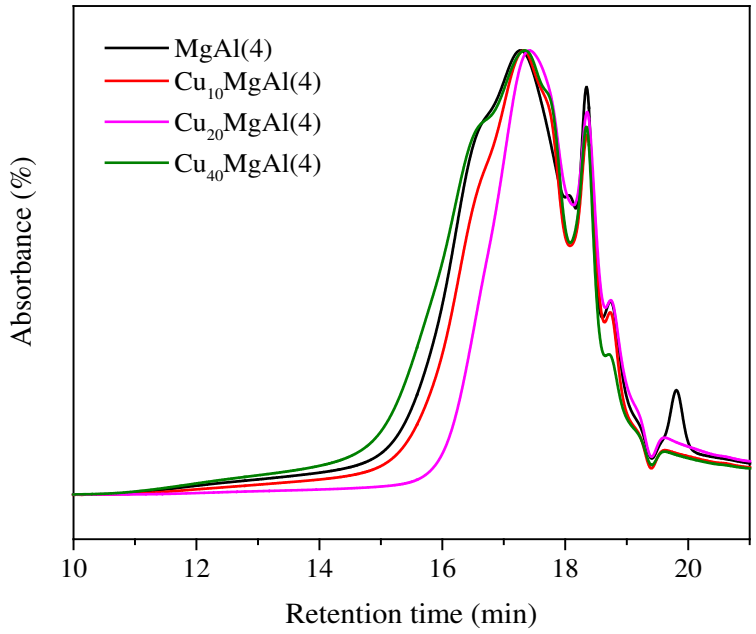

Figure 9. GPC analysis of the THF-insoluble LR obtained from the reaction of lignin in ethanol at 340 °C for 4 h over the mixed oxide catalysts as a function of the Cu content.

Different from the monomers yield trend, the yield of THF-insoluble LR decreased with increasing Cu content (Table 7). This also follows from the analysis of the THF-insoluble LR by GPC (Figure 9). The THF-insoluble LR obtained from reactions using MgAl(4) and

$Cu_{40}MgAl(4)$ as catalysts show higher signals in the early retention time region than the other two catalysts. This indicates that more repolymerized products were formed with these catalysts. Consistent with this, the least repolymerized products were formed with $Cu_{20}MgAl(4)$ as the catalyst (Figure 9). Compared with $Cu_{20}MgAl(4)$, the $Cu_{40}MgAl(4)$ had higher alkylation activity (Table 8), but it yielded more repolymerized products (Table 7 and Figure 9). This can be explained by the lower basicity of this sample, which results in lower activity in Guerbet and esterification reactions. This conclusion is in keeping with the relatively low yield of higher alcohols and esters (Table 7 entries 2 and 4). Compared with the $Cu_{40}MgAl(4)$, $Cu_{10}MgAl(4)$ exhibited very similar activity in Guerbet and esterification reactions, but it gave higher yield of THF-insoluble LR (Table 7 entries 3 and 4). This can be related to the lower alkylation activity of $Cu_{10}MgAl(4)$. From phenol model reactions, we observed that the alkylation degree increased with the Cu content (Table 8). Accordingly, we infer that Cu is pivotal to the high alkylation activity of the hydrotalcites-derived catalysts.

Table 8. Phenol alkylation in ethanol at 340 °C for 4 h over the mixed oxide catalysts with different Cu content.

Catalyst	X (wt%) [a]	Yield of alkylated products (wt%) [a]			Alkylation degree [b]
		mono-alkylated	multi-alkylated	sum	
MgAl(4)	62	41	19	60	2.0
$Cu_{10}MgAl(4)$	65	27	36	63	2.1
$Cu_{20}MgAl(4)$	69	30	34	65	3.4
$Cu_{40}MgAl(4)$	70	24	42	66	5.9

[a] Conversion determined by GC-FID using area normalization method, [b] Determined by ^{1}H-^{13}C HSQC NMR using DMSO d_6 residue peak as internal standard.

All data considered, we can firmly conclude that lignin depolymerization strongly benefits from Guerbet, esterification and alkylation reactions, because these reactions suppress repolymerization of lignin fragments. Among these reactions, the Guerbet and esterification reactions catalyzed by basic sites are more important in suppressing repolymerization than the alkylation reaction catalyzed by Lewis acid sites.

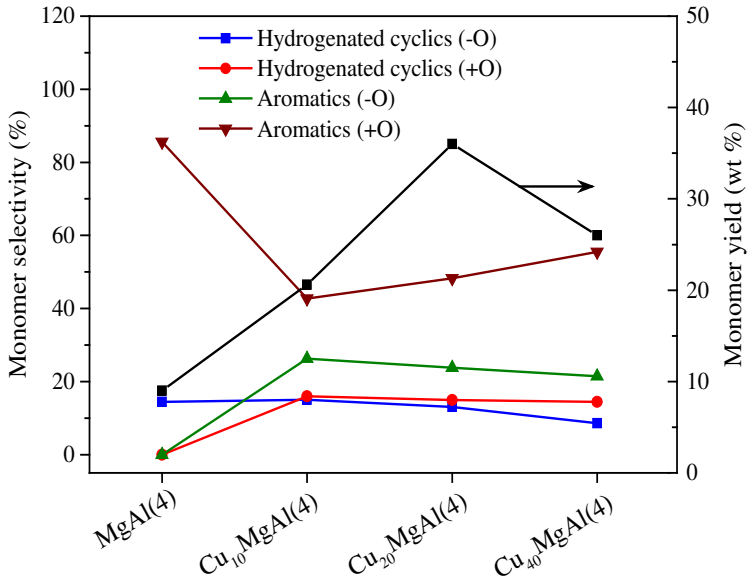

Figure 10. Monomers yield and product distribution after reaction of lignin in ethanol at 340 °C for 4 h over mixed oxide catalysts as a function of the Cu content.

Figure 10 shows how the monomers distribution depends on the Cu content. Without Cu, about 85% of the monomers are oxygenated aromatics. With Cu in the catalyst, the selectivity to oxygenated aromatics is always lower. This difference indicates the important role of Cu in hydrogenation and hydrogenolysis reactions. For the experiment with the Cu-free catalyst, 6.81 mmol of H_2 was formed, which was much lower as compared with the other catalysts (Table S6). In addition to increased H_2 production, the amount of CO, CO_2 and C_1-C_3 alkane and alkene

products in the gas phase were also higher in the presence of Cu. The $Cu_{10}MgAl(4)$ exhibited the highest deoxygenation activity. The fraction of deoxygenated aromatics was 25%. A further increase the Cu content to 40 wt% resulted in decreasing H_2 production and deoxygenation activity. This may be explained by the reduced basicity, as basic sites are involved in ethanol dehydrogenation. Based on these results, we conclude that the combination of Cu and basic sites facilitates dehydrogenation and deoxygenation/hydrogenolysis reactions.

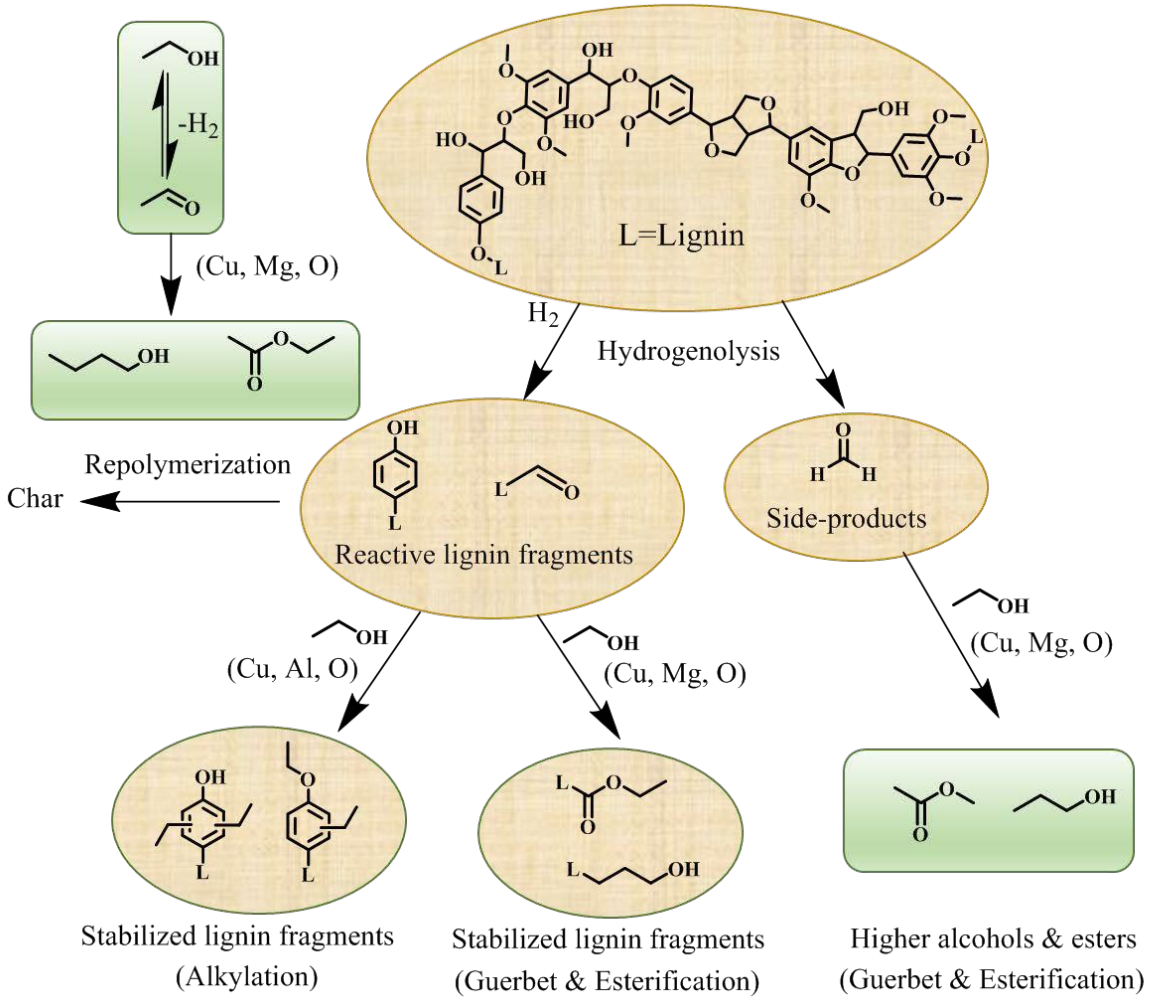

Scheme 1. Proposed reaction network of catalytic depolymerization of lignin in ethanol over the $Cu_xMgAl(y)$ catalysts.

4. CONCLUSION

Scheme 1 summarizes the proposed reaction network and the required active sites for lignin depolymerization in supercritical ethanol over the $Cu_xMgAl(y)$ catalysts. Ethanol is not only a solvent, but also a reactant that participates in the reaction. The ethanol-derived products are mainly C_4-C_8 alcohols and C_4-C_{12} esters produced by Guerbet and esterification reactions. Without catalyst, the main product is char and the yield of aromatic monomers derived from lignin is very low. The combination of Cu and basic sites as well as Lewis acid sites are important for obtaining high monomers yield and low rates of repolymerization during lignin conversion. The combination of Cu and basic sites facilitate the dehydrogenation of ethanol, producing hydrogen needed for hydrogenolysis and hydrodeoxygenation reactions. This results in higher yields of monomers from lignin and also a higher fraction of deoxygenated monomer products. Cu and basic sites also catalyze Guerbet and esterification reactions, producing higher alcohols and esters from ethanol. The higher the activity of the catalyst in Guerbet and esterification reactions is, the less repolymerization products it produces. This can be linked to the scavenging of reactive species such as formaldehyde, which are involved in polymerization reactions of phenolic groups in the products. In addition, the reactive side chains such as aldehyde groups of lignin fragments are also protected by forming new ester and alcohol groups. Such reactions suppress the repolymerization of lignin fragments into high-molecular weight products. The Lewis acid sites due to the presence of Cu and Al catalyze C- and O-alkylation reactions, which lower the reactivity of the phenolic fragments and, in this way, contribute to formation of heavy products. Guerbet and esterification reactions are more important in suppressing repolymerization and char formation than alkylation reactions. Among all evaluated catalysts, the catalyst with 20 wt% Cu derived from a hydrotalcite with a (Cu+Mg)/Al ratio of 4

exhibited the highest activity for Guerbet and esterification reaction as well as nearly optimum alkylation activity. Consistently, it gave the highest monomers yield and the least repolymerization products during soda lignin conversion. With this, we point out that base catalysts with sufficient activity for Guerbet and esterification reactions with alcohols are promising for lignin upgrading into useful aromatics.

Supporting Information available:

Ethanol conversion product (with lignin); Ethanol conversion product list (without lignin); Result of blank reaction (without catalyst); Identification of peaks in HSQC NMR; XPS analysis of the catalysts; GPC analysis of the lignin and its residues; Gas phase products analysis.

This material is available free of charge via the Internet at http://pubs.acs.org.

Acknowledgements

This work was funded by the "New Energy House" project of the Eindhoven Energy Institute in collaboration with the Knowledge and Innovation Community InnoEnergy of the European Institute of Innovations and Technology.

Reference

(1) Zakzeski, J.; Bruijnincx, P. C. A.; Jongerius, A. L.; Weckhuysen, B. M. *Chem. Rev*. **2010**, 110, 3552-3599.

(2) Tuck, C. O.; Perez, E.; Horvath, I. T.; Sheldon, R. A.; Poliakoff, M. *Science* **2012**, 337, 695-699.

(3) Deuss, P. J.; Barta, K. Coord. *Chem. Rev*. **2015**, DOI: 10.1016/j.ccr.2015.02.004

(4) Pandey, M. P.; Kim, C. S. *Chem. Eng. Technol*. **2011**, 34, 29-41.

(5) Rahimi, A.; Ulbrich, A.; Coon, J. J.; Stahl, S. S. *Nature* **2014**, *515*, 249-252.

(6) Barta, K.; Ford, P. C. *Acc. Chem. Res.* **2014**, *47*, 1503-1512.

(7) Ferrini, P.; Rinaldi, R. *Angew. Chem., Int. Ed*. **2014**, 53, 8634-8639.

(8) Parsell, T.; Yohe, S.; Degenstein, J.; Jarrell, T.; Klein, I.; Gencer, E.; Hewetson, B.; Hurt, M.; Kim, J. I.; Choudhari, H.; Saha, B.; Meilan, R.; Mosier, N.; Ribeiro, F.; Delgass, W. N.; Chapple, C.; Kenttamaa, H. I.; Agrawal, R.; Abu-Omar, M. M. *Green Chem*. **2015**, 17, 1492-1499.

(9) Lancefield, C. S.; Westwood, N. J. *Green Chem* **2015**, 17, 4980-4990.

(10) Deuss, P. J.; Scott, M.; Tran, F.; Westwood, N. J.; de Vries, J. G.; Barta, K. *J. Am. Chem. Soc.* **2015**, 137, 7456-7467

(11) Ragauskas, A. J.; Beckham, G. T.; Biddy, M. J.; Chandra, R.; Chen, F.; Davis, M. F.; Davison, B. H.; Dixon, R. A.; Gilna, P.; Keller, M.; Langan, P.; Naskar, A. K.; Saddler, J. N.; Tschaplinski, T. J.; Tuskan, G. A.; Wyman, C. E. *Science* **2014**, 344, 1246843.

(12) Nakamura, T.; Kawamoto, H.; Saka, S. *J. Wood Chem. Technol*. **2007**, 27, 121-133.

(13) Roberts, V. M.; Stein, V.; Reiner, T.; Lemonidou, A.; Li, X. B.; Lercher, J. A. *Chem.-Eur. J*. **2011**, 17, 5939-5948.

(14) Saisu, M.; Sato, T.; Watanabe, M.; Adschiri, T.; Arai, K. *Energy Fuels* **2003**, 17, 922-928.

(15) Bui, V. N.; Laurenti, D.; Delichere, P.; Geantet, C. *Appl. Catal.,* B **2011**, 101, 246-255.

(16) Onwudili, J. A.; Williams, P. T. *Green Chem.* **2014**, 16, 4740-4748.

(17) Zakzeski, J.; Weckhuysen, B. M. *ChemSusChem* **2011**, 4, 369-378.

(18) Lundquis.K; Ericsson, L. *Acta Chem. Scand.* **1970**, 24, 3681-3686.

(19) Okuda, K.; Umetsu, M.; Takami, S.; Adschiri, T. *Fuel Process. Technol.* **2004**, 85, 803-813.

(20) Toledano, A.; Serrano, L.; Labidi, J. *Fuel* **2014**, 116, 617-624.

(21) Hosoya, T.; Kawamoto, H.; Saka, S. *J. Anal. Appl. Pyrolysis* **2008**, 83, 78-87.

(22) Roberts, V. M. *PhD Thesis Tech. Univ. of Munich* **2008**, 120-122

(23) Zhang, J. G.; Asakura, H.; van Rijn, J.; Yang, J.; Duchesne, P.; Zhang, B.; Chen, X.; Zhang, P.; Saeys, M.; Yan, N. *Green Chem.* **2014**, 16, 2432-2437.

(24) Xin, J. N.; Zhang, P.; Wolcott, M. P.; Zhang, X.; Zhang, J. W. *Bioresour. Technol.* **2014**, 155, 422-426.

(25) Xu, W. Y.; Miller, S. J.; Agrawal, P. K.; Jones, C. W. *ChemSusChem* **2012**, 5, 667-675.

(26) Huang, S. H.; Mahmood, N.; Tymchyshyn, M.; Yuan, Z. S.; Xu, C. B. *Bioresour. Technol.* **2014**, 171, 95-102.

(27) Huang, X.; Korányi, T. I.; Boot, M. D.; Hensen, E. J. M. *ChemSusChem* **2014**, 7, 2276-2285.

(28) Ma, R.; Hao, W. Y.; Ma, X. L.; Tian, Y.; Li, Y. D. *Angew. Chem., Int. Ed.* **2014**, 53, 7310-7315.

(29) Barta, K.; Matson, T. D.; Fettig, M. L.; Scott, S. L.; Iretskii, A. V.; Ford, P. C. *Green Chem.* **2010**, 12, 1640-1647.

(30) Wang, X. Y.; Rinaldi, R. *Angew. Chem., Int. Ed.* **2013**, 52, 11499-11503.

(31) Zhao, C.; Kou, Y.; Lemonidou, A. A.; Li, X. B.; Lercher, *J. A. Chem. Commun.* **2010**, 46, 412-414.

(32) Wang, X. Y.; Rinaldi, R. *ChemSusChem* **2012**, 5, 1455-1466.

(33) Wang, X. Y.; Rinaldi, R. *Energy Environ. Sci.* **2012**, 5, 8244-8260.

(34) Zhang, J. G.; Teo, J.; Chen, X.; Asakura, H.; Tanaka, T.; Teramura, K.; Yan, N. *Acs Catal.* **2014**, 4, 1574-1583.

(35) Song, Q.; Wang, F.; Cai, J. Y.; Wang, Y. H.; Zhang, J. J.; Yu, W. Q.; Xu, J. *Energy Environ. Sci.* **2013**, 6, 994-1007.

(36) Ma, R. S.; Xu, Y.; Zhang, X. *ChemSusChem* **2015**, 8, 24-51.

(37) Narani, A.; Chowdari, R. K.; Cannilla, C.; Bonura, G.; Frusteri, F.; Heeres, H. J.; Barta, K. *Green Chem.* **2015**, 17, 4921-4930.

(38) Ma, X.; Ma, R.; Hao, W.; Chen, M.; Yan, F.; Cui, K.; Tian, Y.; Li, Y. *Acs Catal.* **2015**, 5, 4803-4813.

(39) Van den Bosch, S.; Schutyser, W.; Koelewijn, S. F.; Renders, T.; Courtin, C. M.; Sels, B. F. *Chem. Commun.* **2015**, 51, 13158-13161.

(40) Matson, T. D.; Barta, K.; Iretskii, A. V.; Ford, P. C. *J. Am. Chem. Soc.* **2011**, 133, 14090-14097.

(41) Barta, K.; Warner, G. R.; Beach, E. S.; Anastas, P. T. *Green Chem.* **2014**, 16, 191-196.

(42) Van den Bosch, S.; Schutyser, W.; Vanholme, R.; Driessen, T.; Koelewijn, S. F.; Renders, T.; De Meester, B.; Huijgen, W. J. J.; Dehaen, W.; Courtin, C. M.; Lagrain, B.; Boerjan, W.; Sels, B. F. *Energy Environ. Sci.* **2015**, 8, 1748-1763.

(43) Sturgeon, M. R.; O'Brien, M. H.; Ciesielski, P. N.; Katahira, R.; Kruger, J. S.; Chmely, S. C.; Hamlin, J.; Lawrence, K.; Hunsinger, G. B.; Foust, T. D.; Baldwin, R. M.; Biddy, M. J.; Beckham, G. T. *Green Chem.* **2014**, 16, 824-835.

(44) Long, J. X.; Xu, Y.; Wang, T. J.; Yuan, Z. Q.; Shu, R. Y.; Zhang, Q.; Ma, L. *Appl. Energy* **2015**, 141, 70-79.

(45) Singh, S. K.; Ekhe, J. D. *Rsc Adv.* **2014**, 4, 27971-27978.

(46) Singh, S. K.; Ekhe, J. D. *Rsc Adv.* **2014**, 4, 53220-53228.

(47) Huang, X.; Koranyi, T. I.; Boot, M. D.; Hensen, E. J. M. *Green Chem.* **2015**, 17, 4941-4950.

(48) Grob R L.; Barry, E. F. *Modern Practice of Gas Chromatography 4th ed.*; Wiley-Interscience: New Jersey, **2004,** 302-303.

(49) Cavani, F.; Trifirò, F.; Vaccari, A. *Catal. Today* **1991**, 11, 173-301.

(50) Millange, F.; Walton, R. I.; O'Hare, D. *J. Mater. Chem.* **2000**, 10, 1713-1720.

(51) Di Cosimo, J. I.; Diez, V. K.; Xu, M.; Iglesia, E.; Apesteguia, C. R. *J. Catal.* **1998**, 178, 499-510.

(52) Liu, P.; Derchi, M.; Hensen, E. J. M. *Appl. Catal.,* A **2013**, 467, 124-131.

(53) Gosselink, R. J. A. *PhD Thesis Wageningen University* **2011**. 17-23

(54) Sad, M. E.; Neurock, M.; Iglesia, E. *J. Am. Chem. Soc.* **2011**, 133, 20384-20398.

(55) Marcu, I. C.; Tichit, D.; Fajula, F.; Tanchoux, N. *Catal. Today* **2009**, 147, 231-238.

(56) Kozlowski, J. T.; Davis, R. J. *Acs Catal.* **2013**, 3, 1588-1600.

(57) Modrogan, E.; Valkenberg, M. H.; Hoelderich, W. F. *J. Catal.* **2009**, 261, 177-187.

(58) Acevedo, M. D.; Bedogni, G. A.; Okulik, N. B.; Padro, C. L. *Catal. Lett.* **2014**, 144, 1946-1954.

Insert Table of Contents Graphic and Synopsis Here

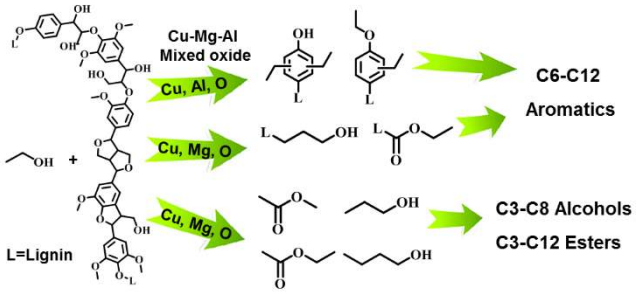

Towards rational catalyst design for lignin conversion